Thermal genesis course and characterization of praseodymium oxide from praseodymium nitrate hydrate

ARTICLE *in* THERMOCHIMICA ACTA · MARCH 2001

Impact Factor: 2.18 · DOI: 10.1016/S0040-6031(00)00727-9

4 AUTHORS, INCLUDING:

Basma Balboul
Minia University
19 PUBLICATIONS **191** CITATIONS

ELSEVIER

Thermochimica Acta 369 (2001) 59–66

thermochimica acta

www.elsevier.com/locate/tca

Thermal genesis course and characterization of praseodymium oxide from praseodymium nitrate hydrate

G.A.M. Hussein[a,*], B.A.A. Balboul[a], M.A. A-Warith[a], A.G.M. Othman[b]

[a]*Chemistry Department, Faculty of Science, Minia University, EI-Minia 60519, Egypt*
[b]*Ceramic Department, National Research Center, Dokki, Cairo, Egypt*

Received 15 June 2000; received in revised form 16 September 2000; accepted 16 September 2000

Abstract

$Pr(NO_3)_3{\cdot}6H_2O$ was used as a precursor to produce $PrO_{1.833}$ at 600°C in an atmosphere of static air. Thermal processes occurred were monitored by means of thermogravimetry, differential thermal analysis and mass spectrometry. IR-spectroscopy and X-ray characterized the intermediates and final solid products. The results showed that, $Pr(NO_3)_3{\cdot}6H_2O$ decomposes through 11 endothermic weight loss processes. Five dehydration steps occurred at 130, 180, 200, 230 and 250°C, leading to the formation of crystalline nitrate monohydrate, Which decomposes to $Pr(NO_3)_2$ at 340°C. The latter, decomposes to $PrO_{1.833}$ at 465°C, via four different intermediates $PrO(NO_3)$ at 430°C, and nonstoichiometric unstable, $PrO_{0.25}(NO_3)_{2.5}$ at 362°C; $Pr(O)_{0.5}(NO_3)_2$ at 382°C and $Pr(O)_{0.75}(NO_3)_{1.5}$ at 400°C. The gaseous decomposition products identified by mass spectroscopy were water vapor and nitrogen oxides (NO, NO_2 and N_2O_5). The activation energy was determined nonisothermally for the thermal processes monitored throughout the decomposition course. The final product $PrO_{1.833}$ has a surface area of 46.3 m^2/g.

Keywords: $Pr(NO_3)_3{\cdot}6H_2O$; $PrO_{1.833}$; Decomposition; Formation; DTA; TG; IR; XRD; Mass spectroscopy

1. Introduction

Praseodymium oxides comprise, Pr_2O_3, PrO_2 plus a range of intermediate phases: Pr_2O_3, $PrO_{1.670}$, $PrO_{1.714}$, $PrO_{1.780}$, $PrO_{1.800}$, $PrO_{1.810}$, and $PrO_{1.833}$ [1–4]. The PrO_2 phase possesses the fluorite structure, while $PrO_{1.810}$, and $PrO_{1.833}$ are oxygen-deficient modifications of fluorite structure. These observed phases depend on the precursor used, and the atmosphere and temperature of decomposition [3–6]. It was also reported [1–4] that, PrO_x is a p-type semiconductor at values of $x < 1.73$ and n-type semiconductor at higher value of x. This behavior was interpreted in the terms of a hopping or electron transfer model involving transfer of electrons between trivalent and tetravalent Pr-ions [1–4].

Several studies [7–14] and review article [6] have been published concerning with the thermal decomposition of rare earth metal salts. It was reported [6] that, rare earth metal oxides obtained from nitrate or acetate precursors leads to higher surface area compared with those obtained from oxalate precursors. Patil et al. [7] reported that, the formation of M_2O_3 from rare earth nitrates takes place via the oxynitrate ($MONO_3$). They also reported the possible formation of anhydrous nitrate, while Wendlandt and Bear [8]

* Corresponding author. Tel.: +20-86-345231; fax: +20-86-342601.
E-mail address: gamalhus@usa.net (G.A.M. Hussein).

0040-6031/01/$ – see front matter
PII: S0040-6031(00)00727-9

stated that the anhydrous nitrates are unstable. Stewart and Wendlandt [9] studied the decomposition of $La(NO_3)_3{\cdot}6H_2O$. They reported that, the dehydration takes place at 105°C to give $La(NO_3)_3{\cdot}3H_2O$, which decomposes at 200°C to form a basic nitrate; and at 500°C, La_2O_3 was the final product. Recently, the decomposition of $Y(NO_3)_3{\cdot}5H_2O$ was studied [10]. It was reported that a thermally stable monohydrate was formed. Also a mixture of $Y(NO_3)_3$ and $Y(OH)(NO_3)_3$ were obtained at 270°C; and $YONO_3$ was detected by XRD as crystalline at 325°C. Y_2O_3 was the final product at 500°C. The texture analysis by nitrogen adsorption method and SEM [11], revealed that Y_2O_3 obtained from $Y(NO_3)_3{\cdot}5H_2O$ at 500°C has a higher surface area ($S_{BET} = 58\ m^2/g$) compared with that obtained at 700°C ($S_{BET} = 20\ m^2/g$). They attribute the lower surface area as results of sintering. Hussein et al [12,13] have studied the decomposition course of $Th(NO_3)_4{\cdot}5H_2O$ [12] and $Dy(NO_3)_3{\cdot}6H_2O$ [13] in air by TG, DTA, IR, XRD and SEM. They reported that, the unhydrous nitrates are thermally unstable and the decompositions gave ThO_2 at 300°C and Dy_2O_3 at 600°C, respectively. Different intermediates of non-stoichiometric oxynitrates were also detected. The $DyONO_3$ is crystalline and thermally stable, compared to $ThO(NO_3)_2$ which is unstable and amorphous. Balboul [14] studied the decomposition course of $Ho(NO_3)_4{\cdot}5H_2O$ in air by TG, DTA, IR, XRD and SEM. It was reported that, the unhydrous nitrates are thermally unstable and the decompositions gave Ho_2O_3 at 560°C. Different intermediates of nonstoichiometric oxynitrates were also detected. The $HoONO_3$ is crystalline and thermally stable.

The present investigation, is intended to characterize the thermal decomposition course of $Pr(NO_3)_3{\cdot}6H_2O$ to the onset of $PrO_{1.833}$ formation. The activation energy (ΔE) was determined nonisothermally for decomposition processes involved. The oxide formed at 600°C was subjected to surface area measurements by N_2 adsorption.

2. Experimental

2.1. Materials

$Pr(NO_3)_3{\cdot}6H_2O$ abbreviated as PrNit, was 99.9% pure (Aldrich, USA). It was used as received. Its calcination products were obtained by heating at various temperatures (200–600°C) for 1 h in a static air. The calcination temperatures were chosen on bases of the thermal analysis results. Prior to analysis, the calcination products were kept dry over silica-gel. For simplicity, these products are donated in the text by PrNit, followed by the calcination temperature. Thus, PrNit-400 indicates decomposition products of PrNit at 400°C for 1 h. The abbreviation WL stands for weight loss.

2.2. Thermal analysis

Thermal analysis were performed using DuPont 9900, Model DTA 951-TG 910 (USA). Thermogravimetry (TG) and differential thermal analysis (DTA) curves were recorded up to 700°C at different heating rates (5–50°C/min.), in static air atmosphere. Equal weights of the test sample (ca. 15 mg) were used in TG measurement. Highly sintered α-Al_2O_3 was the reference material for the DTA measurements.

From the thermoanalytical data, the temperature (T_{max}) obtained from the DTA curve, were determined as a function of the heating rate (θ) applied. The activation energy (ΔE, kJ/mol) was then calculated for each process using Kissinger equation [15].

2.3. Mass spectroscopy

All the mass spectra of the volatile decomposition products were recorded with a Hewlett Packard (HP-5890 series II) gas chromatograph equipped with a 5971 mass selective detector. An HP-vectra Q5/165F data station was used for acquisition and processing of the spectra. Also the data station was equipped with ATLAS for comparison and identification proposes.

The spectra of the gaseous products of PrNit were taken using a sample cell Tekmar 5 ml frit sparger (Pn 14-2337-024). Some modifications were made by making a furnace (coil) surrounding the sample area, with temperature controller. This makes the cell a variable temperature cell.

The standard procedure for automated GC–MS were as follows: powder sample (20 mg) was heated at different temperatures (150–450°C) for 5 min. At each temperature, the gaseous products were trapped using Tekmar LSC2000, dynamic head space concentrator. The trapped products were automatically

desorbed into a HP-5890 GC, interfaced with a 5971A mass-selective detector.

The gaseous decomposition products were injected at 200°C to the GC equipped with 60 m × 0.25 mm DP5 column, with a 2.5 μm film thickness. It is held at 50°C for 10 min after injection, then programmed to 240°C. Helium gas was used as a carrier gas at a flow rate 1.0 ml/min. To prepare for the next experiment (decomposition temperature), the trap (LSC2000) was baked out at 250°C for 10 min under a flow of N_2 gas.

2.4. Infrared spectroscopy

IR spectra were obtained at a resolution 4 cm^{-1} between 4000 and 400 cm^{-1} using a model FT/IR 410 JASCO (Japan). IR spectra of PrNit and its solid calcination products were obtained from thin, lightly loaded (<1%) KBr-supported discs.

2.5. X-ray diffraction

XRD powder patterns were obtained using JSX-60P JEOL diffractometer equipped with Ni-filter and generates a beam of Cu Kα radiation ($\lambda = 1.5418$ Å). The operational settings for all the XRD scans are voltage: 40 kV; current: 30 mA; 2θ = range 4–60°; scanning speed: 8°/min; slit width: 0.02°. For identification purposes the relative intensities (I/I^0) and the *d*-spacing (Å) were compared with standard diffraction patterns of the ASTM powder diffraction files [16].

2.6. Nitrogen adsorption measurements

The N_2 sorption isotherms were determined volumetrically at −196°C using a micro-apparatus based on the design of Lippens et al. [17]. The test sample (PrNit-600) was out-gassed at 200°C for 2 h under evacuation at 10^{-5} Torr.

3. Results and discussions

3.1. Characterization of the decomposition course

3.1.1. Praseodymium nitrate hexahydrate, PrNit, $Pr(NO_3)_3{\cdot}6H_2O$

The DTA curve (Fig. 1) shows an endothermic weight invariant process located at 70°C. A direct visual observation revealed that, the material melts at 69°C. Therefore, process I is due to melting.

3.1.1.1. Processes II–VI. From the TG and DTA curves (Fig. 1), it is clear that processes II–VI are overlapped endothermic weight variant processes, maximizes at 130, 180, 200, 230 and 250°C, respectively. The weight loss associated with each process (Table 1) was close to that which is equivalent to the release of 1 mol of water (i.e. for process II, WL is 4.3% close to that 4.16% theoretically calculated for release of 1 mol of water). Therefore, processes II–VI are most likely proceed as follows:

$$Pr(NO_3)_3 \cdot 6H_2O \overset{130^\circ C}{\rightarrow} Pr(NO_3)_3 \cdot 5H_2O \quad (\text{Step II})$$

$$Pr(NO_3)_3 \cdot 6H_2O \overset{180^\circ C}{\rightarrow} Pr(NO_3)_3 \cdot 4H_2O \quad (\text{Step III})$$

$$Pr(NO_3)_3 \cdot 6H_2O \overset{220^\circ C}{\rightarrow} Pr(NO_3)_3 \cdot 3H_2O \quad (\text{Step IV})$$

$$Pr(NO_3)_3 \cdot 6H_2O \overset{230^\circ C}{\rightarrow} Pr(NO_3)_3 \cdot 2H_2O \quad (\text{Step V})$$

$$Pr(NO_3)_3 \cdot 6H_2O \overset{250^\circ C}{\rightarrow} Pr(NO_3)_3 \cdot H_2O \quad (\text{Step VI})$$

The mass spectra up to 320°C (Fig. 2) is consistent with the TG/DTA data. Only the mass of H_2O (ion 18, at a retention time of 6.8 min.) and its positive radicals, $m/z = 19$, 17 and 16 [18] were detected. In support, the IR spectrum of PrNit-200 (Fig. 3), is very similar to that obtained for untreated PrNit. It displays absorption bands at 1630 cm^{-1} (δOH of HOH) and at 1480, 1420, 1340, 1040, 815 and 740 cm^{-1} due to nitrate groups of a mainly shelving bidentate structure [19,20]. Also, the XRD parttern at 200°C (PrNit200, Fig. 4), revealed the formation of $Pr(NO_3)_3.H_2O$ as a crystalline phase [16].

The corresponding activation energy (Table 1) has values of 54(II), 68 (III), 65(IV), 62(V) and 68(VI) kJ/mol. They are within the range characteristic of dehydration processes [21,22].

3.1.1.2. Process VII. Process VII is an endothermic weight variant process peaking at 340°C. It overlaps with the succeeding processes (VIII–X). The weight loss determined (Table 1) for process VII is 24.40% which is near to that expected 24.8% for the formation of $Pr(NO_3)_3$, as follows:

$$Pr(NO_3)_3 \cdot H_2O \overset{340^\circ C}{\rightarrow} Pr(NO_3)_3 \quad (\text{Step VII})$$

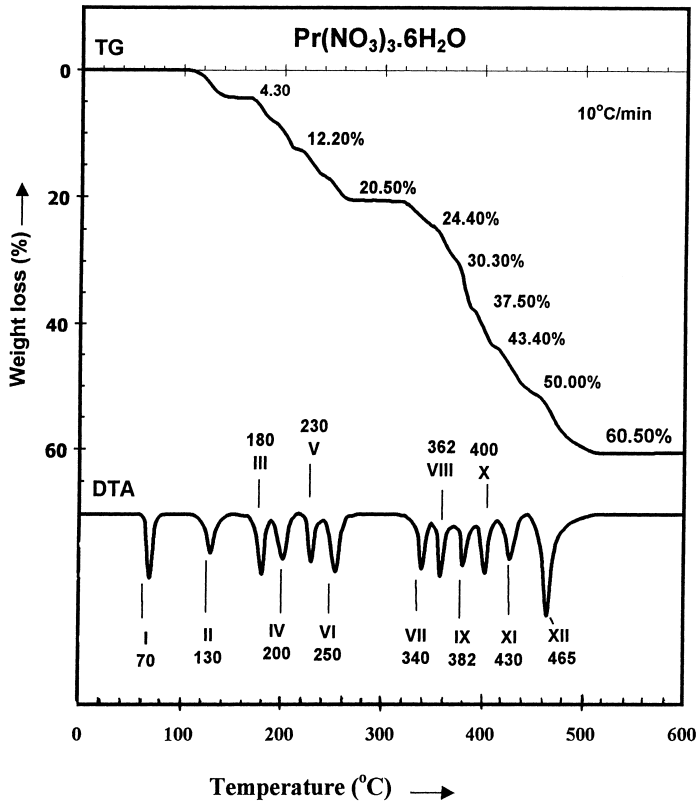

Fig. 1. TG and DTA curves recorded for PrNit at the heating rates indicated, in staticair.

Table 1
Thermal processes, experimental and theoretical Weight losses, composition proposed and activation energy for each process

Process	Observed WL (%)	Theoretical WL (%)	Chemical composition	Activation energy (kJ/mol)
I	–	Melt	$Pr(NO_3)_3{\cdot}6H_2O$	–
II	4.3	4.16	$Pr(NO_3)_3{\cdot}5H_2O$	54
III	8.2	8.31	$Pr(NO_3)_3{\cdot}4H_2O$	68
IV	12.2	12.47	$Pr(NO_3)_3{\cdot}3H_2O$	65
V	16.2	16.63	$Pr(NO_3)_3{\cdot}2H_2O$	62
VI	20.5	20.78	$Pr(NO_3)_3{\cdot}H_2O$	68
VII	24.4	24.8	$Pr(NO_3)_3$	210
VIII	30.3	30.2	$PrO_{0.25}(NO_3)_{2.5}$	199
IX	37.5	37.25	$PrO_{0.5}(NO_3)_2$	205
X	43.4	43.4	$Pr(O)_{0.75}(NO_3)_{1.5}$	212
XI	50.0	49.6	$PrO(NO_3)$	215
XII	60.5	60.8	$PrO_{1.833}$	226

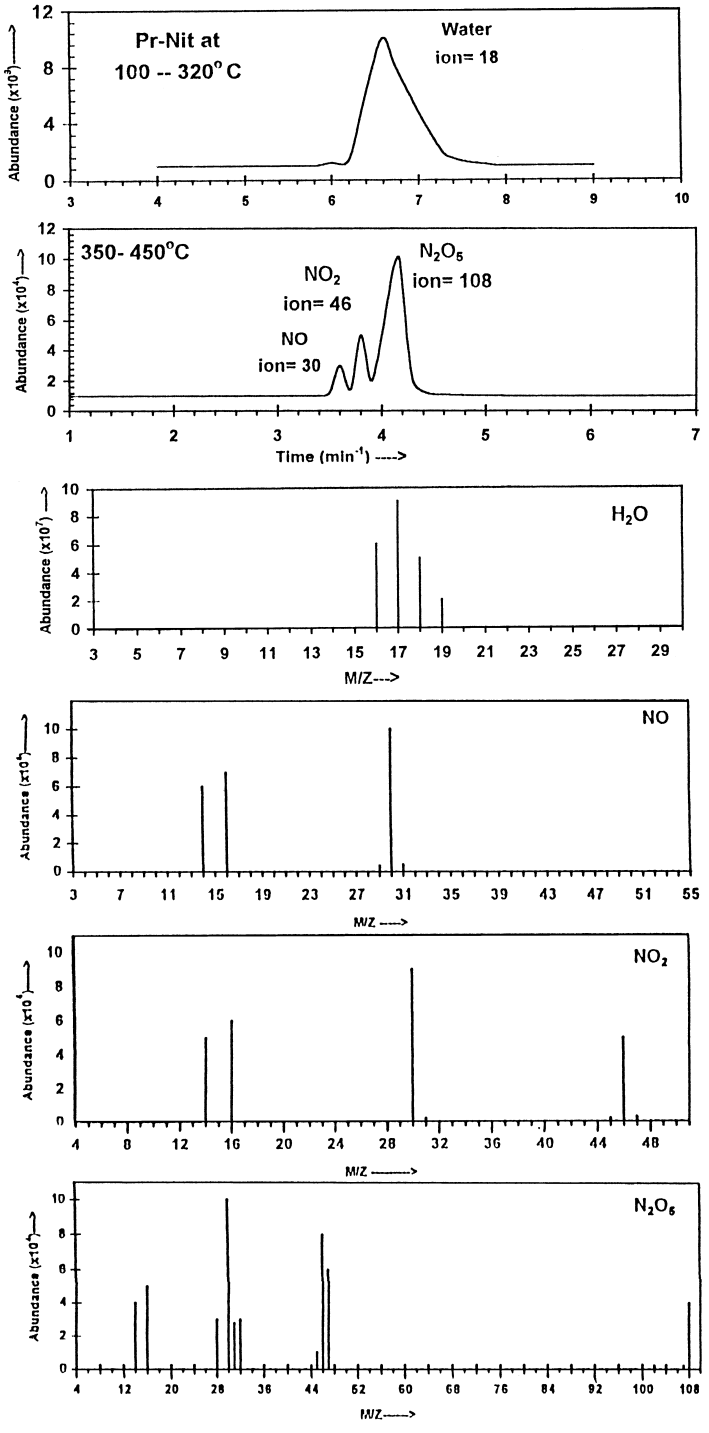

Fig. 2. Mass spectra recorded from the gas surrounding a 20 mg portion of PrNit at the temperatures indicated.

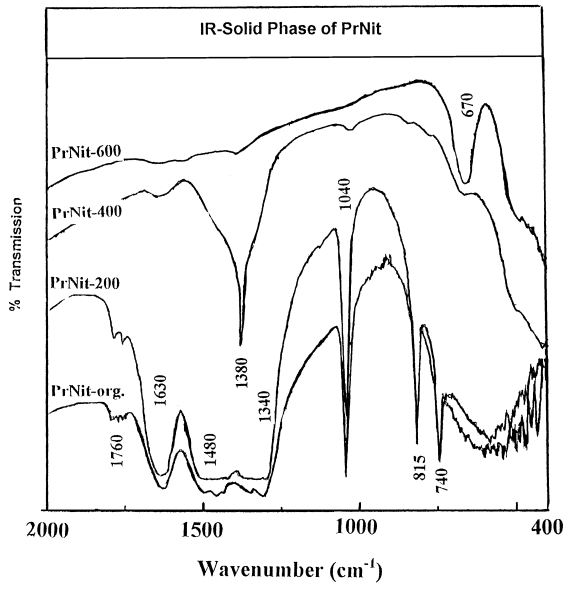

Fig. 3. IR Solid phase spectra for PrNit and its 1 h, calcination products at the temperatures indicated.

The strong overlapping between processes VII and VIII give indication that, anhydrous Pr–nitrate is thermally unstable.

It must be noted that, the anhydrous PrNit was not detected, in agreement with previous studies [8,12,13]. The higher activation energy value (210 kJ/mol) give indication that the removal of the first 5 mol of water is energetically easier than that the removal of the last mol of water. This may give the reason for the thermal stability of the Pr–nitrate monohydrate.

3.1.1.3. Processes VIII–XI. Fig. 1 shows that, processes VIII–XI are strongly overlapped endothermic, maximizes at 362, 382, 400 and 430°C. The weight loss associated with each process (Table 1) was close to that equivalent to the formation of nonstiochoimetric form of oxynitrate, as follows:

$$Pr(NO_3)_3 \overset{362^\circ C}{\rightarrow} PrO_{0.25}(NO_3)_{2.5} + N_2O_5 \quad \text{(Step VIII)}$$

$$PrO_{0.25}(NO_3)_{2.5} \overset{382^\circ C}{\rightarrow} PrO_{0.5}(NO_3)_2 + N_2O_5 \quad \text{(Step IX)}$$

$$PrO_{0.5}(NO_3)_2 \overset{400^\circ C}{\rightarrow} PrO_{0.75}(NO_3)_{1.5} + N_2O_5 \quad \text{(Step X)}$$

$$PrO_{0.75}(NO_3)_{1.5} \overset{430^\circ C}{\rightarrow} PrO(NO_3) + N_2O_5 \quad \text{(Step XI)}$$

The mass spectra up to 450°C, Fig. 2, detects the masses due to N_2O_5 ($m/z = 108$, 47, 46, 45, 32, 31, 30, 28, 16 and 14) [18]. Also NO ($m/z = 30$, 16 and 15) and NO_2 ($m/z = 46$, 30, 16 and 15) were detected as a result of the decomposition of N_2O_5, as follows:

$$N_2O_5 \rightarrow NO + NO_2 + O_2$$

Also the IR spectrum of the solid phase at 400°C (Fig. 3) displays bands mainly due to nitrate [21,22]. However, the evidence for the formation of oxynitrato anion $PrONO_3$, is quite convincing. The composite absorption emerging at 700–400 cm^{-1} is most probably related to Pr–O type vibration [23].

The formation of nonstoichiometric oxynitrate has been reported before [13]. During the decomposition of Dy–nitrate, a different forms of $DyO_x(NO_3)_y$ was formed as an unstable intermediate which decomposed either to oxide or to the higher oxynitrate ($x \gg y$). The similarity between the activation energy values (Table 1) (210 ± 10 kJ/mol) may give the reason for the overlapping with the thermal unstability of these nonstochoimetric forms.

Above 450°C (Fig. 1), the latter $PrONO_3$ decomposes through process X ($T_{max} = 465$°C) to give the final decomposition product $PrO_{1.833}$ (WL determined 60.5% is close to that expected 60.8% form the decomposition of PrNit to $PrO_{1.833}$. The strong support for the formation of $PrO_{1.833}$ was provided by the XRD, Fig. 4, of PrNit-600, which displays only the patterns $PrO_{1.833}$ (ASTM 6-329) [16]. Moreover, the IR spectrum of the solid product at 600°C (Fig. 3), reveals the disappearance of oxynitrate absorptions bands. It displays absorption bands below 800 cm^{-1} due to metal–oxygen vibrations (lattice modes) of (Pr–O) [23]. The activation energy value for process XII is 226 kJ/mol. The higher value of the activation energy may also support the formation of oxygen deficient modification of fluorite structure ($PrO_{1.833}$).

3.1.2. Surface characterization of $PrO_{1.833}$ nitrogen adsorption and surface area measurements

The N_2 adsorption isotherm of PrNit-600 is shown in Fig. 5. The isotherm generally belongs to type IV of the BET classification [24]. The desorption isotherm closed at $P/P^0 > 0.4$, which gives indication that the hysteresis loop is nearly of type H3 [24]. The sorption isotherm and hysteresis loop suggested that the

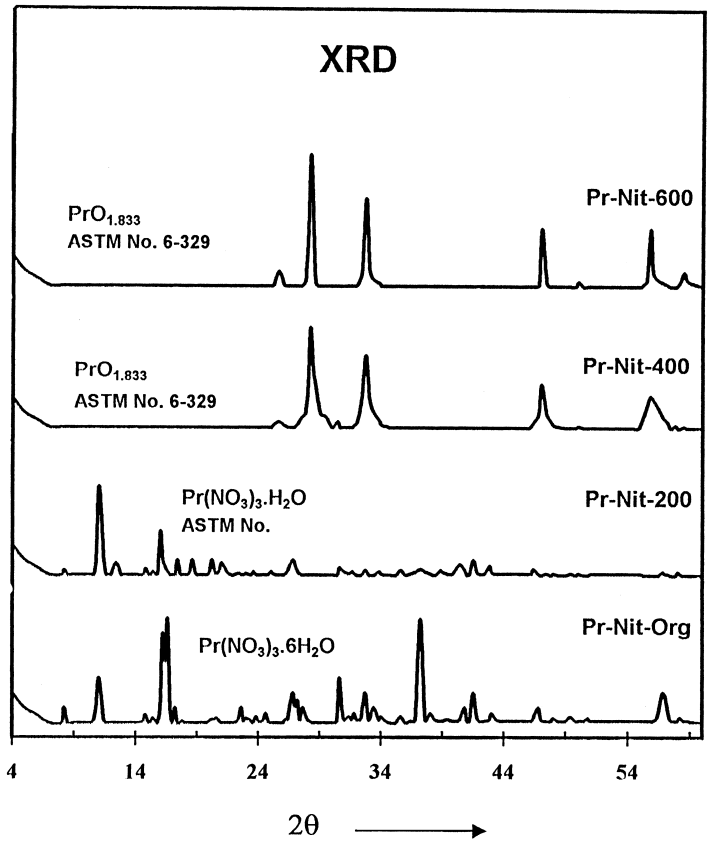

Fig. 4. X-ray powder diffractograms for PrNit and its 1 h calcination products at the temperatures indicated.

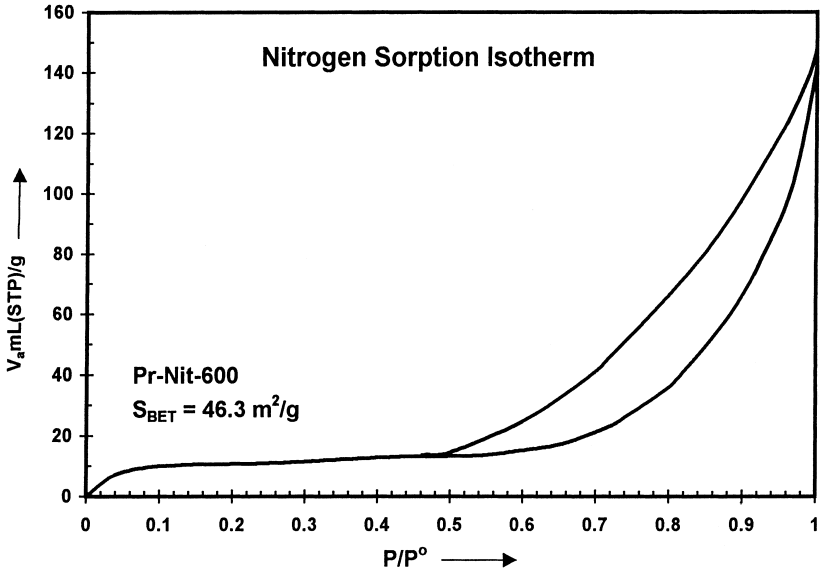

Fig. 5. Nitrogen adsorption isotherm obtained at −195°C (using BET method) for PrNit-600.

surface pores are slit-shaped or interplating [25]. The S_{BET} value determined for PrNit-600 was 46.3 m^2/g.

4. Conclusion

The thermal decomposition of PrNit in atmosphere of air involves the following pathways:

$$Pr(NO_3)_3 \cdot 6H_2O \xrightarrow{130^\circ C} Pr(NO_3)_3 \cdot 5H_2O$$

$$Pr(NO_3)_3 \cdot 6H_2O \xrightarrow{180^\circ C} Pr(NO_3)_3 \cdot 4H_2O$$

$$Pr(NO_3)_3 \cdot 6H_2O \xrightarrow{200^\circ C} Pr(NO_3)_3 \cdot 3H_2O$$

$$Pr(NO_3)_3 \cdot 6H_2O \xrightarrow{230^\circ C} Pr(NO_3)_3 \cdot 2H_2O$$

$$Pr(NO_3)_3 \cdot 6H_2O \xrightarrow{250^\circ C} Pr(NO_3)_3 \cdot H_2O$$

$$Pr(NO_3)_3 \cdot 6H_2O \xrightarrow{340^\circ C} Pr(NO_3)_3$$

$$Pr(NO_3)_3 \cdot 6H_2O \xrightarrow{362^\circ C} PrO_{0.25}(NO_3)_{2.5}$$

$$Pr(NO_3)_3 \cdot 6H_2O \xrightarrow{382^\circ C} PrO_{0.5}(NO_3)_2$$

$$Pr(NO_3)_3 \cdot 6H_2O \xrightarrow{400^\circ C} PrO_{0.75}(NO_3)_{1.5}$$

$$Pr(NO_3)_3 \cdot 6H_2O \xrightarrow{430^\circ C} PrO(NO_3)$$

$$Pr(NO_3)_3 \cdot 6H_2O \xrightarrow{465^\circ C} PrO_{1.833}$$

- The monohydrate of Pr–nitrate is thermally stable, while the unhydrous is unstable.
- No hydroxynitrate was detected as an intermediate.
- A nonstoichiometric form of oxynitrate was detected as an unstable intermediate.
- The gases detected by mass spectroscopy were: H_2O vapor, NO, NO_2, and N_2O_5.
- $PrO_{1.833}$ obtained at 600°C has a surface area of 46.3 m^2/g.

References

[1] P. Kofstad, Nonstoichiometry, Diffusion and Electrical Conductivity in Binary Metal Oxide, Wiley, New York, 1972, p. 289.
[2] Y. Wilbert, A. duquesnoy, F. Marion, C.R. Acad. Sci. (Paris) 263 (1966) 1539.
[3] J.M. Honig, A.F. Clifforf, P.A. Faeth, Inorg. Chem. 2 (1963) 791.
[4] B.G. Hyde, D.J.M. Bevan, L. Eyring, Philos. Trans. R. Soc. London 259 (1966) 583.
[5] G.A.M. Hussein, J. Chem. Soc., Faraday Trans. 90 (1994) 3693.
[6] G.A.M. Hussein, J. Anal. Appl. Pyrol. 37 (1996) 111.
[7] K.C. Patil, R.K. Gosavi, C.N.R. Rao, Inorg. Chem. Acta 1 (1967) 155.
[8] W.W. Wendlandt, J.L. Bear, J. Inorg. Nucl. Chem. 12 (1960) 276.
[9] D.F. Stewart, W.W. Wendlandt, J. Phys. Chem. 63 (1959) 1330.
[10] G.A.M. Hussein, Thermochim. Acta 244 (1994) 139.
[11] H.M. Ismail, G.A.M. Hussein, Powder Technol. 84 (1995) 185.
[12] G.A.M. Hussein, H.M. Ismail, Colloid Surf. 99 (1995) 129.
[13] G.A.M. Hussein, H. Korban, B. Goda, K. Miyaji, Colloid Surf. 125 (1997) 63.
[14] B.A.A. Balboul, Powder Technol. 107 (2000) 168.
[15] H.E. Kissinger, J. Anal. Chem. 29 (11) (1957) 1526.
[16] J.V. Smith (Ed.), X-ray Powder Data File, Amercain Society for Testing and Materials, Philadelphia, USA, 1960.
[17] B.C. Lippens, B.G. Linsen, J.H. de-Boer, J. Catal. 3 (1964) 32.
[18] F.W. Mclafferty, D.B. Stauffer (Eds.), The Wiley/NBS Registry of Mass Spectral Data, Vol. 1, Masses from 2 to 198, New York, 1989.
[19] K. Nakamoto, Infrared Spectra of Inorganic and Coordination Compounds, Wiley, New York, 1970, p. 253.
[20] G.A. Gadsden, Infrared Spectra of Minerals and Related Inorganic Compounds, Butterworths, London, 1975, p. 6511.
[21] M.E. Brown, D. Dollimore, A.K. Galwey, in: C.H. Bamford, C.F.H. Tipper (Eds.), Chemical Kinetics Reactions in the Solid State, Vol. 22, Elsevier, Amsterdam, 1980, p. 130.
[22] G.A.M. Hussein, J. Phys. Chem. 98 (1994) 9657.
[23] J.A. Goldsmith, S.D. Ross, Spectrochem. Acta A 23 (1967) 1909.
[24] S.J. Gregg, K.S.W. Sing, Adsorption Surface Area and Porosity, 2nd Edition, Academic press, London, 1982.
[25] K.S.W. Sing, Pure Appl. Chem. 54 (1982) 2201.